nature catalysis

Article

https://doi.org/10.1038/s41929-022-00844-w

Exploration of the bio-analogous asymmetric C–C coupling mechanism in tandem CO_2 electroreduction

In the format provided by the authors and unedited

Supplementary Information

Exploration of the bio-analogous asymmetric C-C coupling mechanism in tandem CO_2 electroreduction

Chubai Chen, Sunmoon Yu, Yao Yang, Sheena Louisia, Inwhan Roh, Jianbo Jin, Shouping Chen, Peng-Cheng Chen, Yu Shan, Peidong Yang*

*Correspondence to: p_yang@berkeley.edu

Table of Contents

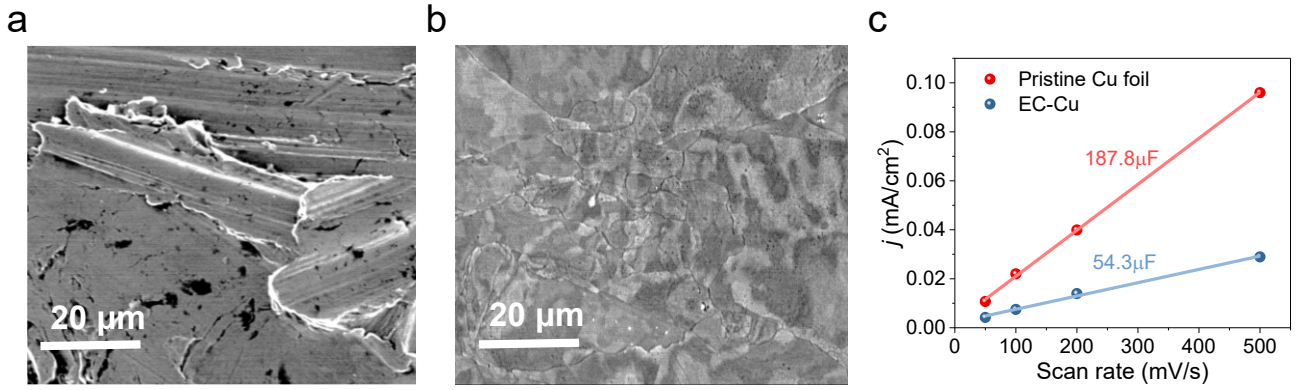

Supplementary Figure 1. Structural characterization of Cu foil before and after electrochemical polish. SEM images of pristine Cu foil (**a**) and Cu foil after electrochemical polish (EC-Cu) (**b**). **c**, Double-layer capacitances of both pristine Cu foil and EC-Cu. Apparently, the surface flatness of Cu foil after electrochemical polish is significantly improved.

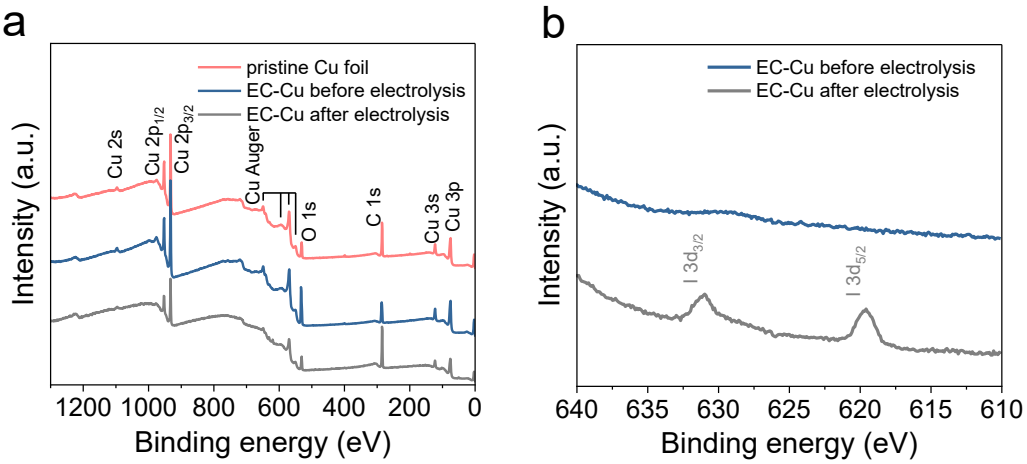

Supplementary Figure 2. Elemental characterization of Cu surface through XPS. **a**, XPS survey of pristine Cu foil, EC-Cu and the EC-Cu after CH_3I related electroreduction experiments. **b**, XPS spectra of I 3d before and after electrolysis.

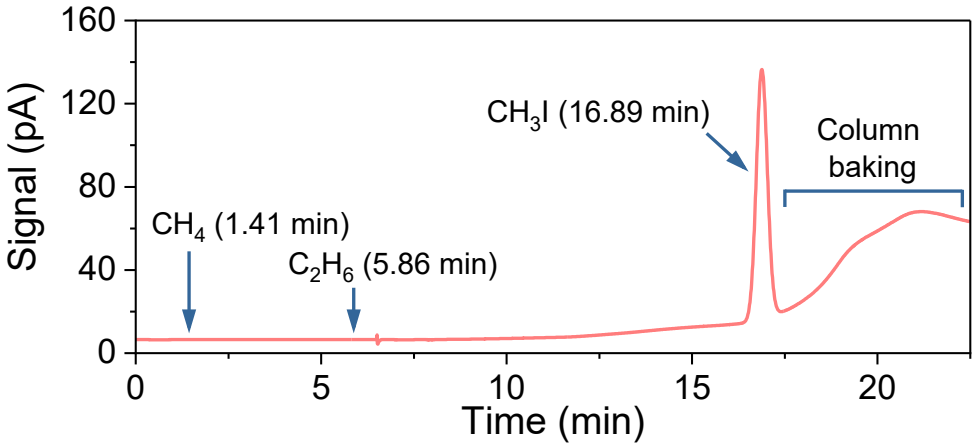

Supplementary Figure 3. Gas effluent composition of CH_3IRR experiments detected by flame ionization detector in gas chromatography under open circuit potential conditions.

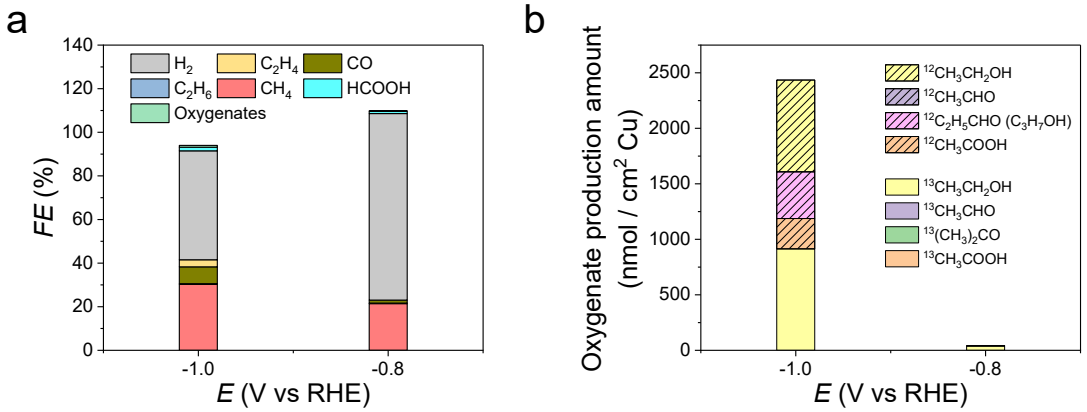

Supplementary Figure 4. a,**b**, Potential dependent product FEs (**a**) and multicarbon oxygenate production amounts after 6 hour electrolysis (**b**) of $^{12}CO_2$ and $^{13}CH_3I$ co-reduction electroreduction on EC-Cu.

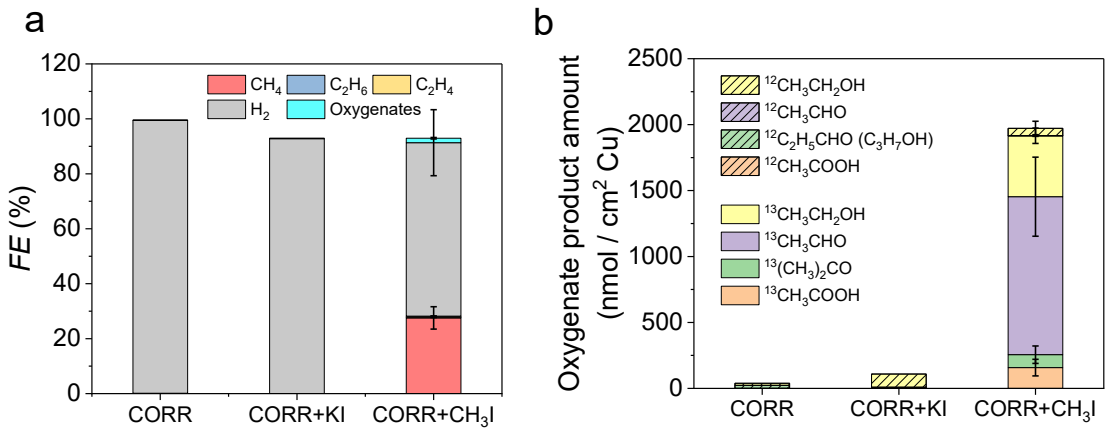

Supplementary Figure 5. a,**b**, Product FEs (**a**) and multicarbon oxygenate production amounts after 6 hour electrolysis (**b**) for the CO electroreduction reaction on EC-Cu with and without 32 mM KI addition, at −0.8 V versus RHE. The product spectrum of ^{12}CO and $^{13}CH_3I$ co-reduction reaction under the same reaction condition was also included for comparison. Error bars represent standard deviations based on three separate experiments, with the center being the mean.

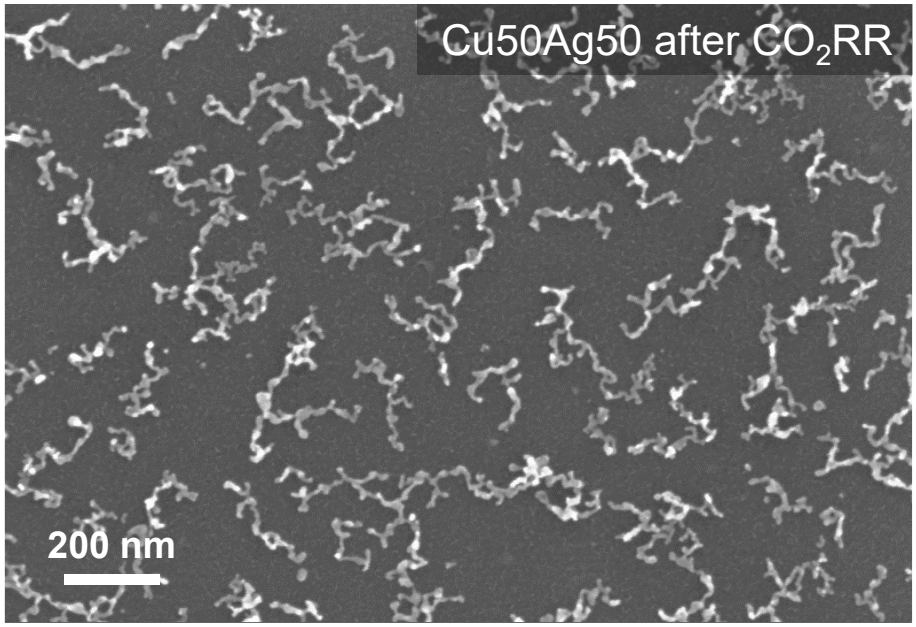

Supplementary Figure 6. SEM image of Cu50Ag50 after CO_2 electrolysis. Based on the SEM image, nanoparticles evolved into dendrite structures.

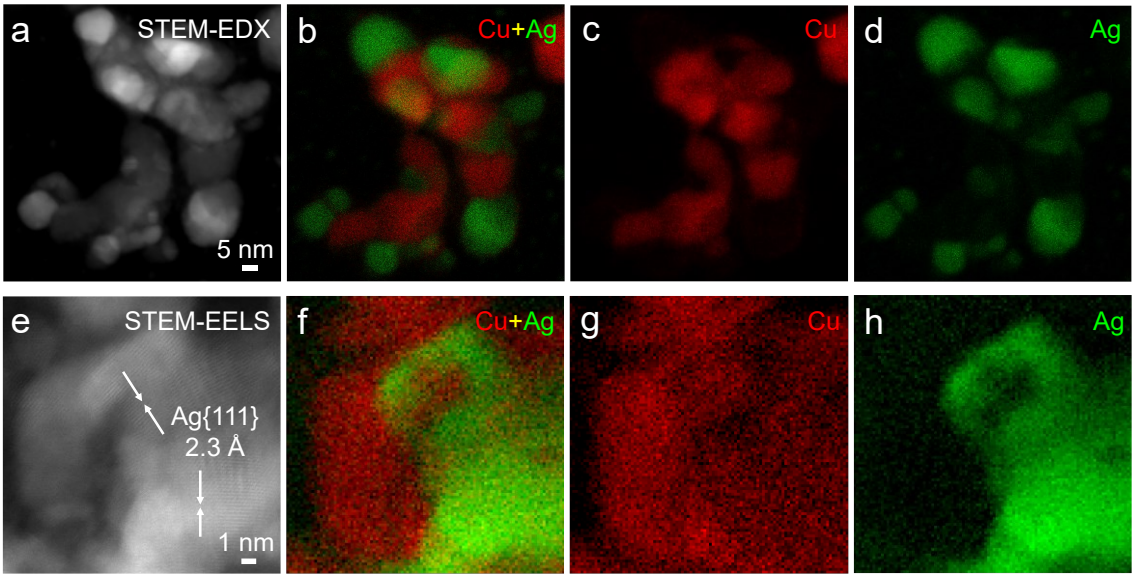

Supplementary Figure 7. Elemental analysis of the dendrite-like nanoparticles formed during CO_2RR. **a-d**, HAADF-STEM image (**a**) and corresponding EDX composite map of Cu (red) and Ag (green) (**b**), Cu map (**c**), and Ag map (**d**), based on the Cu K and Ag L edges. **e-h**, Atomic-scale STEM image with Ag {111} d-spacings labeled by arrows (**e**) and EELS composite maps of Cu and Ag (**f**), Cu map (**g**), and Ag map (**h**), based on Cu L and Ag M edges. Both STEM-EDX and STEM-EELS elemental maps show that Ag nanodomains are embedded in the Cu network in close proximity, which also indicates the significantly higher mobility of Cu during the CO_2RR, relative to isolated Ag domains.

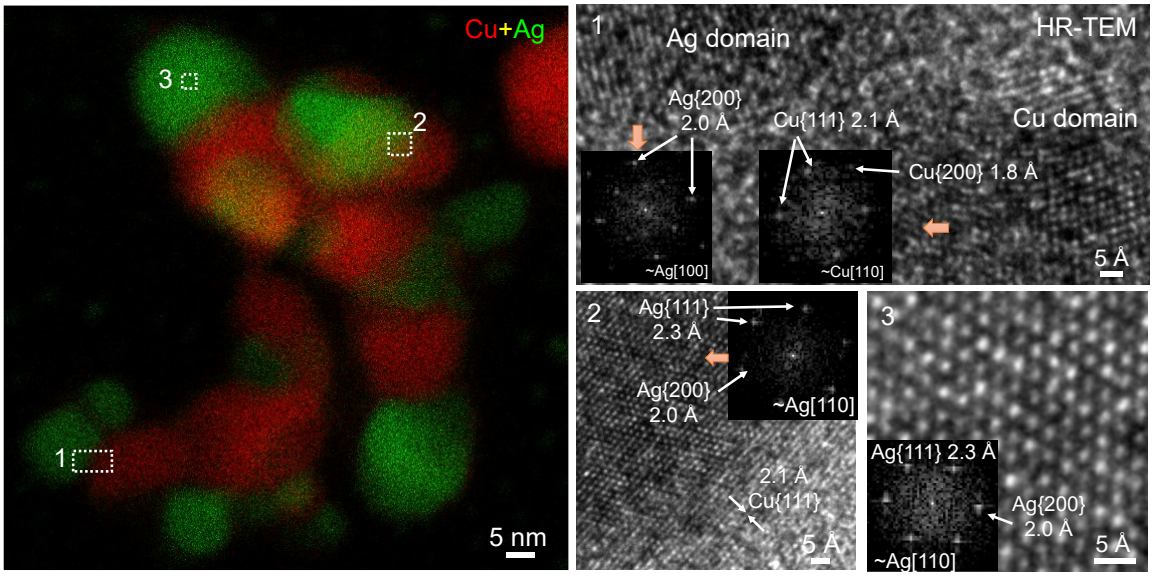

Supplementary Figure 8. HR-TEM images of the representative Ag and Cu nanodomains, corresponding to certain regions in the STEM-EDX elemental maps. Regions 1 and 2 show the interface of Ag and Cu nanodomains, while Region 3 shows a predominant Ag single-crystal domain on the [110] zone axis.

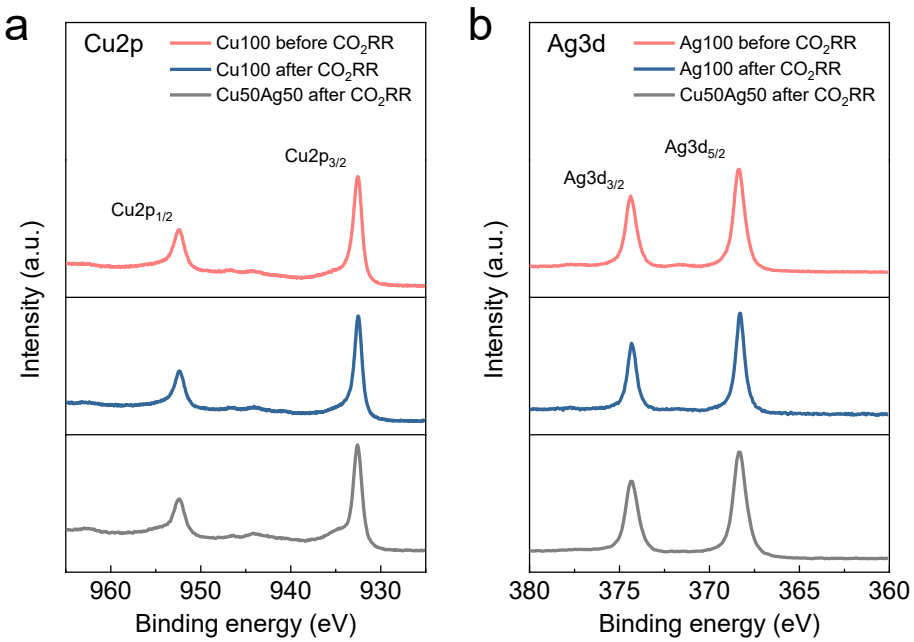

Supplementary Figure 9. a,**b**, XPS spectra of Cu and Ag nanoparticles before and after CO_2 electrolysis. No peak shifting can be found in both Cu (**a**) and Ag (**b**) spectra, which indicates the product spectrum difference in different nanoparticle assemblies is not due to the strong electronic interaction between Cu and Ag.

Supplementary Table 1. Faraday efficiency of Cu-Ag NPs assembly tandem catalysts in CO_2RR

Catalyst	Potential (V vs RHE)[a]	Current (mA)	Faraday Efficiency (FE) (%)							
			H_2	CH_4	CO	C_2H_4	Acetate	CH_3CHO	EtOH	Acetone
Cu100	-1.04	-1.88	38.2	19.9	5.94	9.73	1.72	1.22	2.11	0.19
	-1.18	-7.47	45.6	48.1	0.57	1.87	0.34	0.00	0.55	0.00
	-1.34	-10.5	85.0	16.5	0.15	0.00	0.08	0.00	0.21	0.00
Cu90Ag10	-1.05	-1.05	34.7	5.55	12.5	2.55	2.69	1.09	0.00	0.37
	-1.20	-6.30	12.7	62.2	4.36	7.55	3.36	1.71	4.35	0.59
	-1.33	-11.2	57.8	41.1	0.38	0.48	0.25	0.18	0.50	0.02
Cu50Ag50	-1.04	-1.90	5.51	0.57	53.3	1.37	1.91	1.29	1.50	0.24
	-1.21	-5.31	14.3	39.9	10.7	4.96	2.89	1.22	10.0	0.85
	-1.37	-7.97	37.4	52.7	3.01	2.38	1.32	0.64	3.71	0.09

Catalyst	Potential (V vs RHE)[a]	Faraday Efficiency (FE) (%) *(continued)*							
		Formate	n-PrOH	Glycol aldehyde	MeOH	Allyl alcohol	Hydroxy acetone	Propion aldehyde	Total FE[b]
Cu100	-1.04	10.8	1.05	0.00	0.00	1.12	0.00	0.00	91.6
	-1.18	5.11	0.32	0.00	0.00	0.00	0.00	0.00	102.4
	-1.34	1.22	0.00	0.07	0.05	0.00	0.00	0.00	103.3
Cu90Ag10	-1.05	10.1	1.89	0.00	0.00	2.32	0.00	0.00	73.8
	-1.20	2.70	0.63	0.52	0.06	0.69	0.00	0.27	101.7
	-1.33	1.40	0.00	0.00	0.07	0.00	0.00	0.00	102.2
Cu50Ag50	-1.04	2.61	0.87	0.00	0.00	1.00	0.00	0.00	70.2
	-1.21	2.73	0.95	1.55	0.12	0.74	0.16	0.00	91.0
	-1.37	2.89	0.00	0.85	0.24	0.00	0.00	0.00	105.2

[a.] Applied potentials after iR correction.

[b.] Total FE at low currents tends to be low due to limited gas collection efficiency associated with online GC measurement. As the absolute current value increases, the total FE value improves, eventually reaching 100%. Also, the low total FE at low currents does not mean that there were unidentified gas product species. All the gas products were identified and measured, and thus their FE ratios and production rate ratios are still valid. It should be noted that liquid products were quantified using NMR technique after one-hour CO_2 electrolysis; therefore, liquid product FEs and liquid product production rates must be true values even at low currents.